

---

## **Analyses of structural dynamics revealed flexible binding mechanism for the *Agrilus mali* odorant binding protein 8 towards plant volatiles**

Dexian Li,<sup>ab</sup> Chunbo Li,<sup>ab</sup> and Deguang Liu<sup>ab\*</sup>

\* Correspondence to: College of Plant Protection, Northwest A&F University, Yangling, Shaanxi 712100, China. E-mail: dgliu@nwsuaf.edu.cn

<sup>a</sup> State Key Laboratory of Crop Stress Biology for Arid Areas (Northwest A&F University), Yangling, Shaanxi Province 712100, China

<sup>b</sup> College of Plant Protection, Northwest A&F University, Yangling, Shaanxi Province 712100, China

This article has been accepted for publication and undergone full peer review but has not been through the copyediting, typesetting, pagination and proofreading process which may lead to differences between this version and the [Version of Record](#). Please cite this article as doi: [10.1002/ps.6184](https://doi.org/10.1002/ps.6184)

## Abstract

**BACKGROUND:** Volatiles from host plants are an important source of insect pest attractants and repellents. Insect odorant binding proteins (OBPs) have been widely characterized, but the molecular binding dynamics and underlying mechanisms are still not well understood. Thus, we characterized binding characteristics of AmalOBP8 from the apple buprestid beetle (*Agrilus mali* Matsumura), an unprecedented serious threat to rare apple germplasm resources and local ecosystems.

**RESULTS:** Fluorescence studies demonstrated that the quenching mechanism was clearly static. AmalOBP8 was found to bind with both volatiles at single independent sites. Negative thermodynamic parameters suggested that binding interactions between AmalOBP8 and both volatiles could occur spontaneously. Hydrogen bonding was the key force in AmalOBP8's binding to geranyl formate, for which the amino acid residue Trp106 played a critical role in the binding pocket. Multiple Leu residues in AmalOBP8 created a strong hydrophobic environment, and formed the binding pocket for (*Z*)-3-hexenyl hexanoate. Compared to classic OBPs, in addition to lack of one disulfide bridge, AmalOBP8 had a small  $\alpha$ -helix ( $\alpha 7$ ) at the C-terminus, resulting in greater flexibility and adaptability for this protein to bind with different compound molecules.

**CONCLUSION:** Key residues of AmalOBP8 in binding interactions with plant volatiles were clarified. AmalOBP8 had a large ligand binding spectrum and great flexibility in binding with plant volatiles, providing good molecular targets for screening insect attractants and repellents. Our results can promote understanding of insects' perception of various odorants, and establish a foundation for discovery of new pest control agents.

**Keywords:** olfactory perception; odorant binding proteins; host-plant volatiles; attractant; molecular dynamics; site-directed mutagenesis

Accepted Article

# 1 INTRODUCTION

Modern cultivated apple originates from wild apple, *Malus sieversii*, with intensive recent introgressions from *Malva sylvestris*.<sup>1</sup> Wild apple (*M. sieversii*) in Xinjiang of China is an isolated ecotype with a genetic background that holds great potential for future apple improvement.<sup>1</sup> Recently, the apple buprestid beetle, *Agrilus mali* Matsumara (Coleoptera: Buprestidae), has become the major pest of *M. sieversii*, and 48.6% of the Xinjiang wild apple forest has been damaged by this beetle.<sup>2</sup> In some areas like counties of Xinyuan and Gongliu, most wild apple trees have been destroyed by *A. mali*.<sup>2</sup> Current control strategies are mainly based on larval stage insecticide application through injection and chemical spraying during the short peak period of adult emergence, but such methods have limited control effects, and bring high risks to the fragile local environment.<sup>3,4</sup> Thus, there is an urgent need for development of management strategies from a new perspective.

The olfactory sensation system is of great significance for insects to identify host plants, mates, and ovipositional sites. For example, many insects, such as *Spodoptera littoralis* (Lepidoptera: Noctuidae), *Porphyrophora sophorae* (Hemiptera: Margarodidae), and *Asemum nitidum* (Coleoptera: Cerambycidae), *Bactrocera tryoni* (Diptera: Tephritidae), and *Trichobaris mucorea* (Coleoptera: Curculionidae), can locate and distinguish between different hosts based on plant volatiles.<sup>5-10</sup> Furthermore, host plant volatiles (e.g., hexanal, octanal, nonanal and 1-octen-3-ol) have been successfully used to modulate ovipositional behaviors of insect pests like *Phthorimaea operculella*, and incorporated into management programs.<sup>11</sup> Combinations of host plant volatiles (e.g., linalool, (Z)-3-hexenol, and (Z)-3-hexenyl acetate) and insect pheromones (e.g., 4-methyl-3,5-heptanedione) have been used in early detection and mass trapping of another insect

pest, *Sitona lineatus*.<sup>12</sup> These studies clearly show that natural compounds like host plant volatiles can be used to develop eco-friendly and sustainable measures for management of insect pests. There is evidence that *Agrius planipennis*, which belongs to the same family as our target pest *A. mali*, can be strongly attracted by the green leaf volatile (Z)-3-hexenol.<sup>13</sup> In addition, host volatiles like 2,6-dimethyl-2,4,6-octatriene, geranyl formate, (Z)-3-hexenyl hexanoate, decanal and tetradecanol were shown to be attractive for *A. mali* in our previous studies.<sup>3</sup> Thus, new control means for *A. mali* may be developed, based on the manipulation of its olfactory system.

Insects' olfactory systems are sophisticated and sensitive in perception of host plant volatiles. The initial steps in this process involve an important family of proteins--odorant binding proteins (OBPs).<sup>14</sup> Insect OBPs are small, soluble carrier proteins, which can deliver hydrophobic odorant molecules through the sensillar lymph to the dendritic membrane of olfactory receptor neurons (ORNs). They are usually composed of 120-160 amino acids, and possess a compact structure of  $\alpha$ -helices (six or seven), forming an internal hydrophobic binding cavity.<sup>15, 16</sup> The structure of insect OBPs is further stabilized by three interlocked disulfide bridges between conserved cysteine (Cys) residues.<sup>15, 16</sup> Based on fluorescent competitive binding assays, individual OBPs of many insects (e.g., *Diaphorina citri* and *Acyrtosiphon pisum*) were able to bind a variety of odorant molecules.<sup>17, 18</sup> Binding with external ligands by OBPs can result in action potentials that contribute to subsequent behaviors of insects.<sup>19</sup> However, the molecular dynamics, binding mechanisms and exact physiological functions of insect OBPs are still not well understood.

Nonetheless, OBPs have the potential to be used as targets for the development of eco-friendly pest management techniques. For example, a virtual screening of 1,633 compounds based on ligand structures revealed that thymol acetate, 4-(4-methyl phenyl)-pentanal, thymyl isovalerate, and

*p*-cymen-8-yl had high affinity with *Anopheles gambiae* odorant binding protein 1 (AgamOBP1) and similar properties to DEET (a well-known repellent for mosquitos).<sup>20</sup> Such an approach of reverse chemical ecology relies on the binding capacity of variable ligands to OBPs, which might be optimized by determining their structural features and detailed thermodynamics of binding. Our previous study found that *A. mali* odorant binding protein 8 (AmalOBP8) had high transcription levels on antennae of both sexes, and high binding affinity for two host-plant volatiles (i.e., geranyl formate and (*Z*)-3-hexenyl hexanoate), based on fluorescent binding experiments.<sup>3</sup> In addition, olfactory behavior and field experiments showed that both substances had a relatively good performance in attracting *A. mali*.<sup>21</sup> In this study, multispectral and thermodynamic analyses, molecular simulations, and site-directed mutagenesis will be used to assess the interactions of AmalOBP8 with two host-plant volatiles. We hypothesize that particular structural components (e.g., C-terminus) and residues of AmalOBP8 can be critical in its binding adaptability with plant volatiles. Our results will provide a solid basis for future design, optimization and discovery of novel compounds that can attract or repel *A. mali*.

## 2 MATERIALS AND METHODS

### 2.1 Preparation of recombinant AmalOBP8

The AmalOBP8 protein was expressed and purified using the same method as described in our previous study.<sup>3</sup> Briefly, the recombinant plasmid pET 28a (+)-AmalOBP8 was transferred to *Escherichia coli* BL21 (DE3) competent cells (Weidibio, Shanghai, China). Positive *E. coli* clones were then used as inoculum in LB (Luria-Bertani) liquid medium with ampicillin. The expression of recombinant protein in the bacterial culture was induced by adding

isopropyl- $\beta$ -D-1-thiogalactopyranoside (IPTG, 0.5 mM). The recombinant protein crude was collected and then purified through an affinity chromatography column filled with resin (i.e., Ni NTA Bead 6FF) (Smart-Lifesciences, Changzhou, China). The target protein was verified by SDS-PAGE and finally dialyzed extensively overnight in 20 mmol·L<sup>-1</sup> Tris-HCl buffer (pH 7.4) at 4°C. The concentration of the enriched protein was assayed by using the Bicinchoninic acid (BCA) protein assay kit (CoWinbiotech, Beijing, China), and the protein sample was then stored at -20°C until use.

## 2.2 Fluorescence quenching spectra

A quartz cuvette with a diameter of 1 cm was installed in the F-7000 fluorescence spectrophotometer (Hitachi, Tokyo, Japan), and the slits of both excitation and emission were 5 nm in width. Prior to the assays of fluorescence quenching spectra, the optimal excitation wavelength was determined with spectroscopic scanning for fluorescence excitation. At the optimal excitation wavelength, the emission spectra were recorded at temperatures of 290K and 300K for the AmalOBP8 solution with each host-plant volatile at 0, 5, 10, 15, 20, 25, 30, 35, and 40  $\mu\text{mol}\cdot\text{L}^{-1}$ , respectively. In the experiment, AmalOBP8 was diluted to 1.0  $\mu\text{mol}\cdot\text{L}^{-1}$  with 20 mmol·L<sup>-1</sup> Tris-HCl buffer (pH 7.4), and host plant volatiles [i.e., geranyl formate (CAS NO.: 105-86-2) and (Z)-3-hexenyl hexanoate (CAS NO.: 31501-11-8)] were dissolved with HPLC-grade methanol to generate desired concentrations (see Figure S1 for molecular structures of the two host volatiles).

Stern-Volmer and Lineweaver-Burk equations are used to determine the mechanism of fluorescence quenching caused by protein-small molecule interactions:<sup>22, 23</sup>

$$\frac{F_0}{F} = 1 + K_{sv}[Q] \quad (1)$$

$$\frac{1}{F_0 - F} = \frac{1}{F_0} + \frac{K_D}{F_0[Q]} \quad (2)$$

$F_0$  and  $F$  are the respective fluorescence intensity in the absence and presence of a quencher at a given concentration  $[Q]$ ,  $K_{sv}$  is the Stern-Volmer dynamic quenching constant, and  $K_D$  is the dissociation constant.

Thermodynamic equations were used to assess forces of interactions between AmalOBP8 and two host-plant volatiles:<sup>22, 23</sup>

$$\Delta G = -RT \ln K_A = \Delta H - T\Delta S \quad (3)$$

$$\Delta H = \frac{RT_1T_2 \ln(K_2/K_1)}{T_2 - T_1} \quad (4)$$

$$\Delta S = (\Delta H - \Delta G)/T \quad (5)$$

$\Delta G$ ,  $\Delta S$  and  $\Delta H$  are free energy change, entropy change and enthalpy change, respectively;  $R$  is the ideal gas constant with a value of  $8.314472 \text{ J}\cdot\text{mol}^{-1}\cdot\text{K}^{-1}$ ;  $K_A$  is the apparent association constant, which is reciprocal to  $K_D$ ;  $T_1$  and  $T_2$  represent the two temperatures tested (i.e., 290K and 300K);  $K_1$  and  $K_2$  represent the apparent association constant at each temperature.

### 2.3 UV measurements

A UV-1900 ultraviolet-visible spectrophotometer (Shimadzu, Kyoto, Japan) was used to measure ultraviolet (UV) absorption spectra of AmalOBP8 solution in the presence and absence of host plant volatile components. The recombinant protein was added to a 1 cm standard quartz cuvette at a concentration of  $1.0 \mu\text{mol}\cdot\text{L}^{-1}$ . Then, host plant volatile solutions were added to the protein solution, and the molar concentration ratio of the ligand to the protein was 1: 1. All UV absorption spectra were recorded in a wavelength range of 190-400 nm at 295 K.

### 2.4 Site-directed mutagenesis

The site-directed mutagenesis of AmalOBP8 was conducted according to the manual for the site-directed mutagenesis kit (Vazyme Inc., Nanjing, China). Points of mutations were determined

based on calculations in molecular simulations. Primers used for mutations were listed in Table S1. The mutant AmalOBP8 proteins were expressed with the same method as described above, and fluorescence quenching experiments with mutant proteins were also performed.

## 2.5 Structural modeling of AmalOBP8

Comparative protein structure modeling was performed with Modeller v.9.22 (<https://salilab.org/modeller/>) to obtain the reliable 3D structure of AmalOBP8.<sup>24</sup> Taking the amino acid sequence of AmalOBP8 as a query, the crystal structure for the protein with the highest sequence identity was selected from the Protein Data Bank (<http://rcsb.org/>) as a suitable template for AmalOBP8 modeling.<sup>25</sup> An alignment of the sequence to be modeled with selected templates was conducted. One hundred 3D models of AmalOBP8 was automatically generated in the software. The model with the best MolProbity (<http://molprobity.biochem.duke.edu/>) and Verify 3D (<https://servicesn.mbi.ucla.edu/Verify3D/>) results was chosen as the credible 3D structure of AmalOBP8.<sup>26, 27</sup> The surface hydrophobicity of AmalOBP8 was plotted based on the hydrophobicity of amino acid residues, while the electrostatic potential of the protein surface was calculated by using Coulomb's law.<sup>28</sup> LigPlot+ v.2.1 (<https://www.ebi.ac.uk/thornton-srv/software/LigPlus/>) and Chimera v.1.11 (<http://www.cgl.ucsf.edu/chimera/>) were used to visualize 2D and 3D structures of the proteins, respectively.<sup>28, 29</sup> ESPript v.3.0 (<http://esript.ibcp.fr/ESPript/ESPript/>) was used to visualize alignments of amino acid sequences.<sup>30</sup>

## 2.6 Molecular docking simulations

We used the software AutoDock v.4.2.6 (<http://autodock.scripps.edu/>) to predict the protein-ligand binding properties.<sup>31</sup> The 3D structures of the two volatiles (i.e., geranyl formate and (*Z*)-3-hexenyl

hexanoate) were downloaded from the PubChem database (<https://pubchem.ncbi.nlm.nih.gov/>), and converted to the mol2 format by using OpenBabel v.2.4.1 ([http://openbabel.org/wiki/Main\\_Page](http://openbabel.org/wiki/Main_Page)).<sup>32</sup>

<sup>33</sup> Further chemical properties (e.g., hydrophobicity) of the two volatiles were analyzed with the XLOGP v.3 online tool (<http://www.sioc-ccbq.ac.cn/?p=42&software=xlogp3>).<sup>34</sup> The AMMOS online tool (<https://mobyli.rpbs.univ-paris-diderot.fr/cgi-bin/portal.py>) was used to find the lowest energy conformation of small-molecule compounds.<sup>35</sup> We used the DoGSiteScorer server (<http://www.zbh.uni-hamburg.de/en/servers.html>) to determine the binding pocket in AmalOBP8, which was then used as the molecular docking site.<sup>36</sup> With AutodockTools (v.1.5.6) (<http://autodock.scripps.edu/>), we set the size of docking site at  $60\text{\AA} \times 84\text{\AA} \times 82\text{\AA}$ . The program was run by using the Lamarckian genetic algorithm with the number of runs set at 100, and the maximal number of energy evaluations set at 25000000. Finally, we chose the lowest energy conformation in the largest cluster group for further analyses.

## 2.7 Molecular dynamics (MD) simulations

MD simulations of the AmalOBP8-ligand complex were performed by using Gromacs v.5.1.2 (<https://www.gromacs.org/>).<sup>37</sup> The topology of AmalOBP8 was determined with the commonly used force field GROMOS 54A7, and topologies for ligands was prepared by using Automated Topology Builder v.3.0 (<http://atb.uq.edu.au/register.py>).<sup>38, 39</sup> The 3D structure of the AmalOBP8-ligand complex was immersed in a dodecahedron box with explicit SPC (simple point charge) modeled water molecules extending at least  $10\text{\AA}$  in each direction from the solute, and Cl<sup>-</sup> ions were added to ensure the entire system was in neutral conditions (pH = 7.0). To eliminate unfavorable contacts, the energy of the entire system was minimized by using the steepest-descent algorithm. In the equilibration phase, restraints to the ligand and treatments of temperature coupling

groups were applied. NVT (canonical ensemble) and NPT (isothermal-isobaric ensemble) equilibration of 500 ps each were performed to help the system to reach the desired temperature and pressure. Then, the solvated complex was handled under constant pressure with unrestrained equilibration at 300 K for 5 ns. Upon completion of the equilibration phases, the system was now well equilibrated at the desired temperature and pressure. It was run for 100 ns under the same conditions as the equilibration phase to prevent an abrupt jump in the potential energy. Finally, the energetic contribution of each residue to the binding was calculated by using g\_mmpbsa ([http://rashmikumari.github.io/g\\_mmpbsa/](http://rashmikumari.github.io/g_mmpbsa/)).<sup>40</sup>

### 3 RESULTS

#### 3.1 Fluorescence binding and quenching analyses

If they contain some fluorescent amino acids in high enough concentrations, proteins can fluoresce when excited by the correct wavelength of ultraviolet light. However, when bound to small compound molecules, the intrinsic fluorescence of proteins will often be quenched. Thus, some researchers have started to use fluorescence quenching experiments to gain insight into the binding dynamics of odorant binding proteins with small molecules.<sup>41</sup> Fluorescence excitation spectra showed that the optimal excitation wavelength of UV for AmalOBP8 was 281 nm (Figure S2). Based on the fluorescence emission spectra, the fluorescence intensity of AmalOBP8 decreased with the increase of concentrations of the two host plant volatiles (i.e., geranyl formate and (Z)-3-hexenyl hexanoate), showing direct evidence of binding interactions between the protein and the two ligands. In addition, during the titration of the two volatiles to the AmalOBP8 protein solution, the maximum emission wavelengths did not change significantly. This indicated that the

polarity of the binding site showed little change during interactions between AmalOBP8 and the two host plant volatiles.

The Stern-Volmer and Lineweaver-Burk plots for AmalOBP8-host volatile mixtures were used to explore the quenching mechanism (Figure 1; Table 1). When the value of  $K_{sv}$  increases with increasing temperatures, collision between the fluorophore and the quencher can occur. This kind of quenching is called dynamic or collisional. However, for static quenching,  $K_{sv}$  decreases with increasing temperatures, meaning that a protein-ligand complex is formed between the fluorescent sample and the quencher. The  $K_{sv}$  values for the two host-plant volatiles at 290 K were higher than those at 300 K (Figure 1A, B and Table 1), showing that the binding interactions between AmalOBP8 and the two volatiles were a static process where a ground-state complex between the protein and each volatile could be formed.

We used UV spectroscopy to further clarify the quenching mechanism for the two host plant volatiles. In static quenching, a stable complex is formed between the protein and the ligand, which can cause significant changes in the UV absorption spectra.<sup>42, 43</sup> In this study, as shown in Figure 3, the UV absorption spectra of AmalOBP8 and the protein-ligand complexes did not overlap. This could be attributed to the static quenching caused by formation of a protein-ligand complex, since dynamic quenching would not change the UV absorption spectra. This comparison provided further evidence that quenching of AmalOBP8 by the two volatiles was static.

### **3.2 Three-dimensional structure of AmalOBP8**

Through blast searches, AmalOBP8 showed the highest sequence identity (31%) with *Phormia regina* odorant binding protein 56a (PregOBP56a, PDB ID: 5DIC, resolution = 1.185 Å). Therefore, in order to improve the model quality, the multi-template structural modeling of AmalOBP8 was

conducted. The other templates selected were *Ceratitis capitata* odorant binding protein 22 (CcapOBP22, PDB ID: 6HHE, resolution = 1.516 Å) and *Locusta migratoria* odorant binding protein 1 (LmigOBP1, PDB ID: 4PT1, resolution = 1.65 Å), and they showed a sequence identity of 28% and 22%, respectively, compared with AmalOBP8 (Figure 4B).<sup>15, 44</sup> By using the software Modeller, the final 3D model of AmalOBP8 was constructed and optimized. For all the 114 residues included in the 3D model of AmalOBP8, Ramachandran plots (Figure S3) showed that 98.2% (112/114) of all residues were in favored regions, and 100.0% (114/114) of all residues were in allowed regions. The program Verify 3D can assess the compatibility of an atomic model (3D) and the corresponding amino acid sequence (1D), assign structural classes based on their location and environment (alpha, beta, loop, polar, nonpolar, and etc.), and compare the resulting structure to valid ones in databases.<sup>27</sup> A reasonable model requires that at least 80% of all the amino acid residues score above 0.2. Our modeling results showed that 100% of AmalOBP8 residues scored above 0.2 (Figure S4). The Ramachandran plots and Verify 3D scores indicated the good quality of the constructed AmalOBP8 model.

### 3.3 Analyses of molecular dynamics

The putative binding pocket (shown by a yellow grid area) was identified in the 3D model of AmalOBP8 (Figure S5). AmalOBP8-ligand complexes were generated by docking the two host plant volatiles into the binding pocket, respectively. The root mean square deviation (RMSD) of the simulated structure over time was used to verify the stability of molecular dynamics simulations. In the course of 100 ns MD simulations, AmalOBP8-ligand complexes could be optimized, and reach the equilibrium (Figure 5). The values of root mean square fluctuation (RMSF) reflect the flexibility and local motion characters of secondary structure elements of a protein when binding with a ligand.

Accepted Article

It is clear in Figure 4 that the 3D model of AmalOBP8 is composed of  $\alpha$ -helices and free loops. In Figures 5G and 5H, relatively sharp peaks of RMSF correspond to loops between  $\alpha$ -helices in the 3D structure of AmalOBP8. It was evident that loop regions were much more flexible than  $\alpha$ -helix regions. The radius of gyration ( $R_g$ ) maintained a relatively steady value, showing that the protein was stably folded during the simulation (Figures 5E, 5F). Parameters of RMSD, RMSF and  $R_g$  for the 100 ns MD simulations indicate the stability of AmalOBP8-ligand complexes, and the quality of the AmalOBP8 model.

### 3.4 Identification of key molecular forces in binding of AmalOBP8

As shown in Table 1, in all cases,  $\Delta G$  values were negative, indicating that interactions between AmalOBP8 and the two host volatiles were a spontaneous process. The interactions between proteins and small compound molecules usually include hydrogen bonds, van der Waals interactions, hydrophobic interactions and electrostatic forces. Based on the values of  $\Delta H$  and  $\Delta S$ , the above-mentioned forces of molecular interactions can be distinguished:  $\Delta H < 0$  and  $\Delta S < 0$  represent the occurrence of major forces of hydrogen bonds and van der Waals; typical hydrophobic interactions are shown by positive enthalpy and entropy ( $\Delta H > 0$  and  $\Delta S > 0$ );  $\Delta H < 0$  and  $\Delta S > 0$  indicate the occurrence of hydrophobic and electrostatic interactions. In our study, negative values of  $\Delta H$  and  $\Delta S$  indicated that binding interactions between AmalOBP8 and geranyl formate could be mainly driven by forces of hydrogen bonding and van der Waals. However, binding interactions between AmalOBP8 and (Z)-3-hexenyl hexanoate were mainly hydrophobic (shown by  $\Delta H > 0$  and  $\Delta S > 0$ ).

In the simulation analyses, the binding pocket of AmalOBP8 for geranyl formate included residues Leu30, Ser31, His32, Gly34, Phe35, Trp46, Trp106, and Thr109 (Figure 7A). Among these,

the H atom from -NH group of Trp106 formed a hydrogen bond with the O atom of geranyl formate. In addition, the N atom in the indole group of Trp106 remained at a close distance (an average of 3.73 Å) to the O atom in geranyl formate in 100 ns simulations (Figure S6). As shown in Figure 6, hydrogen bonding between AmalOBP8 and geranyl formate did not always remain the same across 100 ns MD simulations. The average number of hydrogen bonds between AmalOBP8 and geranyl formate was 0.42, and even reached 4 at some instant (Figure 6A). In addition, analyses of protein molecular surface of hydrophobicity (Figure 7C: white) and electrostatic potential (Figure 7E: mostly white) around the binding pocket showed that hydrophobic and electrostatic interactions had only very limited roles in the binding of AmalOBP8 with geranyl formate.

In the simulation analyses of AmalOBP8's binding with (*Z*)-3-hexenyl hexanoate, a hydrophobic binding pocket was formed with residues Leu10, Leu50, Leu53, Val55, Leu62, Val67, Leu79, Cys104, Tyr105 and Thr108 (Figure 7B). Compared with geranyl formate, the average number of hydrogen bonds formed between the protein and (*Z*)-3-hexenyl hexanoate was very low (only 0.05) (Figure 6), showing that hydrogen bonding was unlikely to play important roles in binding of AmalOBP8 with (*Z*)-3-hexenyl hexanoate. Hydrophobic residues of Leu's formed a strong hydrophobic environment (orange red) around (*Z*)-3-hexenyl hexanoate (Figure 7D), and electrostatic interactions (white) between the protein and was weak (Figure 7F).

We further investigated hydrophobic properties (i.e., logP) of the two host-plant volatiles with XLOGP. Values of logP, that is the logarithm of n-octanol/water partition coefficient of a substance, reflect the distribution of the substance in the two phases of oil and water. The larger the logP value, the more hydrophobic the substance.<sup>34</sup> The logP values of (*Z*)-3-hexenyl hexanoate and geranyl formate were 3.8 and 3.5, respectively. This result indicates that a more hydrophobic environment is

needed to stabilize the binding of (*Z*)-3-hexenyl hexanoate during its transportation, consistent with the abovementioned thermodynamics simulations.

We also calculated the free energy of binding between AmalOBP8 and the two host volatiles to further evaluate the binding interactions involved. As shown in Table 2, the AmalOBP8 binding free energies for geranyl formate and (*Z*)-3-hexenyl hexanoate were -24.64 kJ/mol and -23.18 kJ/mol, respectively. The theoretical calculations were very close to  $\Delta G$  obtained by fluorescence quenching (Table 1). The energy combinations of hydrophobic interactions, hydrogen bonds, and van der Waals forces were -32.13 kJ/mol and -34.39 kJ/mol for binding of AmalOBP8 with geranyl formate and (*Z*)-3-hexenyl hexanoate, respectively. The role of electrostatic interactions was relatively small in the binding of AmalOBP8 with both geranyl formate (-2.01 kJ/mol) and (*Z*)-3-hexenyl hexanoate (-1.21 kJ/mol), consistent with the results of the electrostatic potential map (Figure 7E, 7F). However, upon the disappearance of forces of hydrogen bonding, the electrostatic forces might be critical for interaction between AmalOBP8 and geranyl formate. Compared to geranyl formate (7.49 kJ/mol), a larger torsional energy needs to be overcome for AmalOBP8's binding with (*Z*)-3-hexenyl hexanoate (11.21 kJ/mol).

The molecular mechanics–Poisson–Boltzmann surface area (MM-PBSA) method was used to perform the analyses of per-residue free energy decomposition for MD simulations (Table 3). For geranyl formate, residues Trp106, Tyr105, Tyr46 and Gly34 played key roles in the binding interactions, and their contributions were -2.84 kJ/mol, -2.37 kJ/mol, -2.11 kJ/mol, -2.11 kJ/mol, respectively. The amino acid residue with the largest energy contribution was Trp106. This residue could form hydrogen bonds in binding of AmalOBP8 with geranyl formate. Although it was not involved in formation of the binding pocket, Tyr105 was close to the key residue Trp106. So, it is

not surprising that Tyr105 also showed a relatively large energy contribution. In the complex formed by AmalOBP8 and (*Z*)-3-hexenyl hexanoate, the four amino acid residues with highest energy contributions were all leucine, and Leu79 contributed the most (i.e., -3.39 kJ/mol), showing the importance of leucine residues in forming a hydrophobic binding cavity.

### 3.5 Site-directed mutagenesis of AmalOBP8

To further verify the results of molecular dynamics simulations, the key residues (i.e., Trp106 and Leu79) were mutated in AmalOBP8 to Ala with only one methyl group in the side chain. Using the fluorescence quenching technique mentioned above, we measured the binding capacity of AmalOBP8-mW106A with geranyl formate, as well as the binding capacity of AmalOBP8-mL79A with (*Z*)-3-hexenyl hexanoate.

Upon the replacement of Trp106 by Ala in AmalOBP8,  $\Delta S$  of the mutant protein became positive, compared with negative values for the wild-type protein (Table 1). This indicated that hydrogen bonding between the mutant protein and geranyl formate could not occur. On the other hand, hydrophobic and electrostatic forces became the main binding forces between the mutant protein and geranyl formate. Thus, hydrogen bonds between the atom N of Trp106 indolyl and the atom O from the geranyl formate are essential for high binding ability of native AmalOBP8 for geranyl formate. However, after Leu79 of the protein was mutated to Ala, binding interactions between the AmalOBP8 mutant and (*Z*)-3-hexenyl hexanoate showed little change, and hydrophobic interactions were still the main binding force. We also noticed that  $K_{SV}$  values of mutant proteins no longer decreased with increasing temperatures (Table 1), indicating that the quenching mechanism turned dynamic from forming a stable protein-ligand complex.

## 4 DISCUSSION

Sensitive perception of plant volatiles is critical for insects in location of host plants, mates, and ovipositional sites. In the olfactory signal transduction process, the first initial steps involve the binding of external odorant molecules by insect OBPs, for which the molecular dynamics and underlying mechanisms are still not well understood. In order to understand insects' recognition and discrimination of host odors, many studies have used fluorescence competitive binding bioassays, often providing an incomplete picture of binding interactions involved.<sup>3,41</sup> Thus, in this study, we conducted additional fluorescence quenching assays to assess the binding dynamics of two host plant volatiles (i.e., geranyl formate and (*Z*)-3-hexenyl hexanoate) with AmalOBP8 from *A. mali* (a serious threat to the existence of wild apple forests in Tianshan Mountains). These assays showed direct evidence of binding interactions between the protein and the two ligands. The binding interactions between AmalOBP8 and the two volatiles were found to be a static process, where a ground-state complex between the protein and each volatile could be formed.

In the molecular modeling, AmalOBP8 showed a seventh  $\alpha$ -helix at its C-terminus (Figure 4), unlike classic insect OBPs with six  $\alpha$ -helices.<sup>45,46</sup> Some OBPs can form a small seventh  $\alpha$ -helix, which enters the binding pocket to stabilize the structure when the ligand is released.<sup>47</sup> Interestingly, in our simulations of molecular dynamics, the seventh  $\alpha$ -helix of AmalOBP8 was quickly transformed into a loop structure upon binding with geranyl formate. However, when binding with (*Z*)-3-hexenyl hexanoate, the seventh  $\alpha$ -helix of AmalOBP8 remained the form of helix instead of a loop structure. Secondary structure changes were also reported in the binding process of DhelOBP21 with (+)- $\beta$ -pinene, where the amino-terminus of the protein was transformed from random coil to an  $\alpha$ -helix to cover the binding pocket.<sup>48</sup> Such results indicate

that insect OBPs may be able to increase their binding flexibility and spectra through modification of secondary structures.

The binding flexibility and spectra of insect OBPs can also be closely related to the number of disulfide bridges and the characteristics of binding cavity. The structure of many insect OBPs is stabilized by the presence of three interlocked disulfide bridges, which confer only limited flexibility to the structure, thus providing protection against thermal denaturation and degradation by proteolytic enzymes.<sup>47</sup> AmalOBP8, a minus-C OBP, has only four conserved cysteine residues, forming two of disulfide bridges between  $\alpha$ -helices [one:  $\alpha$ 1 and  $\alpha$ 3 (Cys17-Cys48); the other:  $\alpha$ 5 and  $\alpha$ 6 (Cys86-Cys104)]. Similarly, *Batocera horsfieldi* OBPM2 has only two disulfide bonds, and forms a large binding pocket; this protein has been shown to have extensive binding flexibility with a larger binding spectrum compared with classic OBPs.<sup>49</sup> Higher flexibility of such structures may add the adaptability of the seventh  $\alpha$ -helix in binding between proteins and ligands. In our case, AmalOBP8 also had continuous ligand binding channels with a volume of 1638.78 Å<sup>3</sup> (Figure S5), and our previous research showed that AmalOBP8 had the ability to bind more diverse kinds of ligands, compared with a classic OBP (i.e., AmalOBP3).<sup>3</sup> Thus, an additional helix (i.e., the seventh) in minus-C OBPs like AmalOBP8 may add flexibility to their binding with small molecules, providing more adaptability in insects' perception of olfactory signals.

The binding capacity of insect OBPs with host plant volatiles can be ultimately attributed to many molecular forces like hydrogen bonding, hydrophobic interactions and van der Waals. We found that binding interactions between AmalOBP8 and geranyl formate could be mainly driven by hydrogen bonding, where Trp106 was the key amino acid residue in the binding cavity. However, hydrogen bonding between AmalOBP8 and geranyl formate did not always remain the same across

100 ns MD simulations. Similar dynamics was found in the binding of *Grapholita molesta* PBP2 (pheromone binding protein 2) with (Z)-8-dodecenyl acetate, where hydrogen bonds had a length between 2.7 and 3.0 Å with random disappearance.<sup>50</sup> The critical role of Trp106 (or hydrogen bonding) of AmalOBP8 was further confirmed with experiments of site-directed mutagenesis. On the other hand, in our study, binding interactions between AmalOBP8 and (Z)-3-hexenyl hexanoate were found to be mainly hydrophobic, and hydrophobic residues of Leu's (i.e., Leu10, Leu50, Leu53, Leu62 and Leu79) formed a strong hydrophobic environment in the binding cavity. Similarly, *Apolygus lucorum* OBP22 could bind to plant terpenoids with a similar hydrophobic pocket composed of multiple hydrophobic amino acids (e.g., Leu5, Ile40, Met41, and Val44).<sup>51</sup> Thus, both hydrophobic interactions and hydrogen bonding could play key roles in insects' perception of host volatiles.

AmalOBP8 was found to be abundantly expressed in the antennae of *A. mali*, indicating its significance in odorant perception of this serious pest.<sup>3</sup> Analyses of per-residue free energy decomposition from MD simulations indicated key roles of residues like Trp106 and Leu79 of AmalOBP8 in perception of host volatiles in *A. mali*, further showing AmalOBP8's potential to be used as a molecular target in management of *Agrilus* pests. Based on calculations of molecular dynamics, excellent ligands can be identified or designed for important proteins for various purposes.<sup>52, 53</sup> For example, analyses of binding between AgamOBP1 and DEET showed that larger aromatic groups (e.g., indole or naphthalene ring) could be accommodated, and have  $\pi$ - $\pi$  interactions with Trp114, resulting in the finding that 4-methyl-1-(1-oxodecyl)-piperidine (modified from DEET) had stronger binding ability with AgamOBP1.<sup>54</sup> In another study, adding a hydrophilic group to a particular position of 1-dodecanol could facilitate its interaction with *Cydia pomonella*

pheromone binding protein 2, thus providing a foundation for development of biologically more active compounds.<sup>55</sup> Similarly, based on analyses of structural dynamics in our study, it is likely to enhance hydrogen bonding with Trp106 through adding hydrogen bond acceptor groups to geranyl formate [e.g., addition of -OH gives (*E*)-3,7-dimethylocta-2,6-dien-1-yl hydrogen carbonate (Figure S7A)]. In order to increase hydrophobic interactions with multiple Leu residues in AmalOBP8, we can also modify (*Z*)-3-hexenyl hexanoate through replacing the =O group with non-polar -CH<sub>3</sub> [i.e., generation of (*Z*)-2-(hex-3-en-1-yloxy) heptane] (Figure S7B). Such modifications still need further verification studies in the future, nonetheless, our results provide a starting point and solid foundation for high-throughput screening of highly effective attractants or repellents for management of *A. mali*.

## 5 CONCLUSION

In summary, comprehensive analyses of binding characteristics of two volatiles with AmalOBP8 were achieved by using fluorescence spectrometry, UV spectrometry, site-directed mutagenesis, and molecular simulations. Our results demonstrated that the quenching mechanism of the involved AmalOBP8-ligand formation was clearly static and the binding process was spontaneous. The stability of AmalOBP8-ligand complexes could be attributed to hydrogen bonds (involving the amino acid residue Trp106) or hydrophobic interactions (involving leucine residues like Leu79). Thus, thermodynamics of binding interactions and key sites involved in insect OBPs can be very different for different volatiles, showing flexibility of insect OBP's binding with volatiles and complexity in insects' perception of olfactory signals. Our results also suggest that insect OBPs like AmalOBP8, which lack a pair of disulfide bonds and contain an additional  $\alpha$ -helix

Accepted Article

at the C-terminus, can have a larger ligand binding spectrum and greater flexibility in binding with small molecules, thus playing critical roles in insects' perception of variable plant volatiles. Thus, the results have clearly corroborated our hypothesis that particular structural components (e.g., the additional  $\alpha$ -helix at the C-terminus) and residues of insect OBPs can be critical in their adaptability in binding with plant volatiles. Insect OBPs like AmalOBP8 may be used as a molecular target for screening for insect attractants and repellents from diverse plant volatiles of insect hosts. For this purpose, further computational and structural studies are needed to determine the exact conformational changes in OBP-ligand complexes. Our study provides insights into the flexibility and selectivity of insect OBPs' binding with small molecules of olfactory information, as well as the underlying mechanisms.

## **ACKNOWLEDGEMENTS**

We would like to thank Xiaoning Cui and Keke Sun (Northwest A&F University) for their field and lab help. This study was funded by the National Natural Science Foundation of China (U1803107 and U1503102).

## **CONFLICT OF INTEREST**

The authors declare that the research was conducted in the absence of any commercial or financial relationships that could be construed as a potential conflict of interest.

## **SUPPORTING INFORMATION**

Supporting information (Figures S1-S7 and Table S1) can be found in the online version of this

Accepted Article

article.

## REFERENCES

- 1 Duan N, Bai Y, Sun H, Wang N, Ma Y, Li M *et al.*, Genome re-sequencing reveals the history of apple and supports a two-stage model for fruit enlargement. *Nat Commun* **8**:249 (2017).
- 2 Cao LM, Zhang YL, van Achterberg C, Wang ZY, Wang XY, Zhao WX *et al.*, Notes on braconid wasps (Hymenoptera, Braconidae) parasitising on *Agrilus mali* Matsumura (Coleoptera, Buprestidae) in China. *Zookeys* **867**:97-121 (2019).
- 3 Cui X, Liu D, Sun K, He Y, and Shi X, Expression profiles and functional characterization of two odorant-binding proteins from the apple buprestid beetle *Agrilus mali* (Coleoptera: Buprestidae). *J Econ Entomol* **111**:1420-1432 (2018).
- 4 Bozorov TA, Rasulov BA, and Zhang D, Characterization of the gut microbiota of invasive *Agrilus mali* Matsumura (Coleoptera: Buprestidae) using high-throughput sequencing: uncovering plant cell-wall degrading bacteria. *Sci Rep* **9**:4923 (2019).
- 5 Conchou L, Anderson P, and Birgersson G, Host plant species differentiation in a polyphagous moth: olfaction is enough. *J Chem Ecol* **43**:794-805 (2017).
- 6 Liu XF, Chen HH, Li JK, Zhang R, Turlings TC, and Chen L, Volatiles released by Chinese liquorice roots mediate host location behaviour by neonate *Porphyrophora sophorae* (Hemiptera: Margarodidae). *Pest Manag Sci* **72**:1959-64 (2016).
- 7 Collignon RM, Swift IP, Zou Y, McElfresh JS, Hanks LM and Millar JG. The influence of host plant volatiles on the attraction of longhorn beetles to pheromones. *J Chem Ecol* **42**:215-229 (2016).
- 8 Cunningham JP, Carlsson MA, Villa TF, Dekker T and Clarke AR. Do Fruit ripening volatiles enable resource specialism in polyphagous fruit flies? *J Chem Ecol* **42**:931-940 (2016).
- 9 Lee G, Joo Y, Diezel C, Lee EJ, Baldwin IT and Kim SG. *Trichobaris* weevils distinguish amongst toxic host plants by sensing volatiles that do not affect larval performance. *Mol Ecol* **25**:3509-3519 (2016).
- 10 Bruce TJ and Pickett JA. Perception of plant volatile blends by herbivorous insects-finding the right mix. *Phytochemistry* **72**:1605-11 (2011).
- 11 Anfora G, Vitagliano S, Larsson MC, Witzgall P, Tasin M, Germinara GS *et al.*, Disruption of *Phthorimaea operculella* (Lepidoptera: Gelechiidae) oviposition by the application of host plant volatiles. *Pest Manag Sc* **70**:628-35 (2014).
- 12 St Onge A, Cárcamo HA, and Evenden ML, Evaluation of semiochemical-baited traps for monitoring the pea leaf weevil, *Sitona lineatus* (Coleoptera: Curculionidae) in field pea crops. *Environ Entomol* **47**:93-106 (2018).
- 13 Silk P, Mayo P, Ryall K, and Roscoe L, Semiochemical and communication ecology of the emerald ash borer, *Agrilus planipennis* (Coleoptera: Buprestidae). *Insects* **10**:323 (2019).
- 14 Brito NF, Moreira MF, and Melo AC, A look inside odorant-binding proteins in insect chemoreception. *J Insect Physiol* **95**:51-65 (2016).
- 15 Falchetto M, Ciossani G, Scolari F, Di Cosimo A, Nenci S, Field LM *et al.*, Structural and biochemical evaluation of *Ceratitis capitata* odorant-binding protein 22 affinity for odorants involved in intersex communication. *Insect Mol Biol* **28**:431-443 (2019).
- 16 Li TT, Liu WC, Zhu J, Yang YH, Ma C, Lu C *et al.*, Crystal structure and ligand identification of odorant binding protein 4 in the natural predator *Chrysopa pallens*. *Int J Biol Macromol* **141**:1004-1012 (2019).

- 17 Qin YG, Yang ZK, Song DL, Wang Q, Gu SH, Li WH *et al.*, Bioactivities of synthetic salicylate-substituted carboxyl (E)- $\beta$ -Farnesene derivatives as ecofriendly agrochemicals and their binding mechanism with potential targets in aphid olfactory system. *Pest Manag Sci* **76**:2465-2472 (2020).
- 18 Zhang H, Chen JL, Lin JH, Lin JT, and Wu ZZ, Odorant-binding proteins and chemosensory proteins potentially involved in host plant recognition in the Asian citrus psyllid, *Diaphorina citri*. *Pest Manag Sci* **76**:2609-2618 (2020).
- 19 Gadenne C, Barrozo RB, and Anton S, Plasticity in insect olfaction: to smell or not to smell? *Annu Rev Entomol* **61**:317-33 (2016).
- 20 da Costa KS, Galúcio JM, da Costa CHS, Santana AR, Dos Santos Carvalho V, do Nascimento LD *et al.*, Exploring the potentiality of natural products from essential oils as inhibitors of odorant-binding proteins: a structure- and ligand-based virtual screening approach to find novel mosquito repellents, *ACS Omega* **4**:22475-22486 (2019).
- 21 Cui X, Behavioral responses of *Agrilus mali* to host-plant volatiles and function of related olfactory genes, *Northwest A & F University* (2018).
- 22 Li QL, Yi SC, Li DZ, Nie XP, Li SQ, Wang MQ *et al.*, Optimization of reverse chemical ecology method: false positive binding of *Aenasius bambawalei* odorant binding protein 1 caused by uncertain binding mechanism. *Insect Mol Biol* **27**:305-318 (2018).
- 23 Tan J, Song X, Fu X, Wu F, Hu F, and Li H, Combinatorial multispectral, thermodynamics, docking and site-directed mutagenesis reveal the cognitive characteristics of honey bee chemosensory protein to plant semiochemical. *Spectrochim Acta A Mol Biomol Spectrosc* **201**:346-353 (2018).
- 24 Webb B and Sali A, Comparative protein structure modeling using MODELLER. *Curr Protoc Bioinformatics* **54**:5.6.1-5.6.37 (2016).
- 25 Burley SK, Berman HM, Kleywegt GJ, Markley JL, Nakamura H, and Velankar S, Protein data bank (PDB): the single global macromolecular structure archive. *Methods Mol Biol* **1607**:627-641 (2017).
- 26 Williams CJ, Headd JJ, Moriarty NW, Prisant MG, Videau LL, Deis LN, Verma V, Keedy DA, Hintze BJ, Chen VB, Jain S, Lewis SM, Arendall WB 3rd, Snoeyink J, Adams PD, Lovell SC, Richardson JS, and Richardson DC, MolProbity: More and better reference data for improved all-atom structure validation. *Protein Sci*; **27**(1):293-315(2018).
- 27 Bowie JU, Lüthy R, and Eisenberg D, A method to identify protein sequences that fold into a known three-dimensional structure. *Science* **253**:164-70(1991).
- 28 Pettersen EF, Goddard TD, Huang CC, Couch GS, Greenblatt DM, Meng EC *et al.*, UCSF Chimera--a visualization system for exploratory research and analysis. *J Comput Chem* **25**:1605-12 (2014).
- 29 Laskowski RA, and Swindells MB. LigPlot+: multiple ligand-protein interaction diagrams for drug discovery. *J Chem Inf Model* **51**:2778-86 (2011).
- 30 Robert X and Gouet P. Deciphering key features in protein structures with the new ENDscript server. *Nucleic Acids Res* **42**:W320-W324 (2014).
- 31 Morris GM, Huey R, Lindstrom W, Sanner MF, Belew RK, Goodsell DS *et al.*, AutoDock4 and AutoDockTools4: automated docking with selective receptor flexibility. *J Comput Chem* **30**:2785-91 (2009).
- 32 Kim S, Chen J, Cheng T, Gindulyte A, He J, He S *et al.*, PubChem 2019 update: improved

- access to chemical data. *Nucleic Acids Res* **47**:D1102-D1109 (2019).
- 33 O'Boyle NM, Banck M, James CA, Morley C, Vandermeersch T, and Hutchison GR. Open Babel: an open chemical toolbox. *J Cheminform* **3**:33 (2011).
- 34 Cheng T, Zhao Y, Li X, Lin F, Xu Y, Zhang X *et al.*, Computation of octanol-water partition coefficients by guiding an additive model with knowledge. *J Chem Inf Model* **47**:2140-8 (2007).
- 35 Pencheva T, Lagorce D, Pajeva I, Villoutreix BO, and Miteva MA, AMMOS: automated molecular mechanics optimization tool for in silico screening. *BMC Bioinformatics* **9**:438 (2008).
- 36 Volkamer A, Kuhn D, Rippmann F, and Rarey M, DoGSiteScorer: a web server for automatic binding site prediction, analysis and druggability assessment. *Bioinformatics* **28**:2074-5 (2012).
- 37 Pronk S, Páll S, Schulz R, Larsson P, Bjelkmar P, Apostolov R *et al.*, GROMACS 4.5: a high-throughput and highly parallel open source molecular simulation toolkit. *Bioinformatics* **29**:845-54 (2013).
- 38 Schmid N, Eichenberger AP, Choutko A, Riniker S, Winger M, Mark AE *et al.*, Definition and testing of the GROMOS force-field versions 54A7 and 54B7. *Eur Biophys J* **40**:843-56 (2011).
- 39 Stroet M, Caron B, Visscher KM, Geerke DP, Malde AK, and Mark AE, Automated topology builder version 3.0: prediction of solvation free enthalpies in water and hexane. *J Chem Theory Comput* **14**:5834-5845 (2018).
- 40 Kumari R, Kumar R, Open Source Drug Discovery Consortium, and Lynn A, g\_mmpbsa--a GROMACS tool for high-throughput MM-PBSA calculations. *J Chem Inf Model* **54**:1951-62 (2014).
- 41 Yi SY, Li DZ, Zhou CX, Tang YL, Abdelnabby HE, and Wang MQ, Screening behaviorally active compounds based on fluorescence quenching in combination with binding mechanism analyses of SspOBP7, an odorant binding protein from *Sclerodermus sp.* *Int J Biol Macromol* **107**:2667-2678 (2018).
- 42 Fu XB, Zhang YL, Qiu YL, Song XM, Wu F, Feng YL *et al.*, Physicochemical basis and comparison of two type II sex pheromone components binding with pheromone-binding protein 2 from tea geometrid, *Ectropis obliqua*. *J Agric Food Chem* **66**:13084-13095 (2018).
- 43 Nivens D A, Zhang Y and Angel S M. Detection of uranyl ion via fluorescence quenching and photochemical oxidation of calcein. *J Photoch Photobio A* **152**:167-173 (2002).
- 44 Zheng J, Li J, Han L, Wang Y, Wu W, Qi X *et al.*, Crystal structure of the *Locusta migratoria* odorant binding protein. *Biochem Biophys Res Commun* **456**:737-42 (2015).
- 45 Northey T, Venthur H, De Biasio F, Chauviac FX, Cole A, Ribeiro KA Junior *et al.*, Crystal structures and binding dynamics of odorant-binding protein 3 from two aphid species *Megoura viciae* and *Nasonovia ribisnigri*. *Sci Rep* **6**:24739 (2016).
- 46 Gonzalez D, Rihani K, Neiers F, Poirier N, Fraichard S, Gotthard G *et al.*, The *Drosophila* odorant-binding protein 28a is involved in the detection of the floral odour  $\beta$ -ionone. *Cell Mol Life Sci* **77**:2565-2577 (2020).
- 47 Pelosi P, Mastrogiovanni R, Iovinella I, Tuccori E, and Persaud KC, Structure and biotechnological applications of odorant-binding proteins. *Appl Microbiol Biotechnol* **98**:61-70 (2014).
- 48 Yang RN, Li DZ, Yu G, Yi SC, Zhang Y, Kong DX *et al.*, Structural transformation detection contributes to screening of behaviorally active compounds: dynamic binding process analysis

- of DhelOBP21 from *Dastarcus helophoroides*. *J Chem Ecol* **43**:1033-1045 (2017).
- 49 Zheng ZC, Li DZ, Zhou A, Yi SC, Liu H, and Wang MQ, Predicted structure of a Minus-C OBP from *Batocera horsfieldi* (Hope) suggests an intermediate structure in evolution of OBPs. *Sci Rep* **6**:33981 (2016).
- 50 Tian Z, Li Y, Xing Y, Li R, and Liu J, Structural insights into two representative conformations of the complex formed by *Grapholita molesta* (Busck) pheromone binding protein 2 and Z-8-Dodecenyl Acetate. *J Agric Food Chem* **67**:4425-4434 (2019).
- 51 Liu H, Duan H, Wang Q, Xiao Y, Wang Q, Xiao Q *et al.*, Key amino residues determining binding activities of the odorant binding protein AlucOBP22 to two host plant terpenoids of *Apolygus lucorum*. *J Agric Food Chem* **67**:5949-5956 (2019).
- 52 Śledź P and Caflisch A. Protein structure-based drug design: from docking to molecular dynamics. *Curr Opin Struct Biol* **48**:93-102 (2018).
- 53 Dong L, Shen S, Chen W, Xu D, Yang Q, Lu H *et al.*, Discovery of novel inhibitors targeting human O-GlcNAcase: docking-based virtual screening, biological evaluation, structural modification, and molecular dynamics simulation. *J Chem Inf Model* **59**:4374-4382 (2019).
- 54 Tsitsanou KE, Thireou T, Drakou CE, Koussis K, Keramioti MV, Leonidas DD *et al.*, *Anopheles gambiae* odorant binding protein crystal complex with the synthetic repellent DEET: implications for structure-based design of novel mosquito repellents. *Cell Mol Life Sci* **69**:283-97 (2012).
- 55 Tian Z, Li Y, Zhou T, Ye X, Li R, Liu J *et al.*, Structure dynamics reveal key residues essential for the sense of 1-dodecanol by *Cydia pomonella* pheromone binding protein 2 (CpomPBP2). *Pest Manag Sci* (2020).

**Table 1. Fluorescence quenching constants <sup>a</sup> and thermodynamic parameters for binding of wild-type (WT) and mutant AmalOBP8 with two host plant volatiles**

AmalOBP8 - ligand	Temperature (K)	K <sub>sv</sub> (× 10 <sup>4</sup> L/mol)	K <sub>D</sub> (μmol/L)	K <sub>a</sub> (× 10 <sup>4</sup> L/mol)	ΔG (kJ/mol)	ΔH (kJ/mol)	ΔS (J/mol/K)	Major binding forces
WT - geranyl formate	290	1.64±0.03	18.24±3.09	5.60±1.04	-27.22	-32.38	-17.79	Hydrogen bonds and Van der Waals interactions
	300	1.27±0.01	11.66±3.02	9.05±2.74	-28.33		-13.48	
WT - (Z)-3-hexenyl hexanoate	290	1.60±0.02	14.30±2.95	7.19±1.48	-27.82	14.47	138.96	Hydrophobic interactions
	300	1.32±0.01	16.99±1.80	5.93±0.60	-27.39		132.89	
W106A - geranyl formate	290	1.04±0.11	32.13±4.73	3.15±0.43	-25.81	-4.46	73.59	Hydrophobic and electrostatic forces
	300	1.05±0.11	30.21±6.34	3.40±0.64	-25.96		71.65	
L79A - (Z)-3-hexenyl hexanoate	290	1.08±0.01	27.40±5.53	3.75±0.77	-26.20	2.10	97.60	Hydrophobic interactions
	300	1.17±0.01	28.20±6.37	3.68±0.93	-26.13		94.10	

Note: <sup>a</sup> Derived from Stern-Volmer and Lineweaver-Burk equations; W106A, Trp106 mutated to Ala; L79A, Leu79 mutated to Ala.

**Table 2. Estimation of free energy (kJ/mol) for binding of AmalOBP8 with two volatiles**

Energy categories	Geranyl formate	(Z)-3-hexenyl hexanoate
Final intermolecular energy <sup>a</sup>	-32.13	-34.39
VdW + Hbond + desolv <sup>b</sup>	-30.12	-33.18
Electrostatic energy	-2.01	-1.21
Final total internal energy	-1.84	-2.89
Torsional free energy	7.49	11.21
Unbound system's energy <sup>c</sup>	-1.84	-2.89
Estimated free energy <sup>d</sup>	-24.64	-23.18

<sup>a</sup> Final intermolecular energy is equal to the sum of electrostatic forces, hydrophobic interactions, hydrogen bonds, and van der Waals interactions; <sup>b</sup> VdW, Hbond, and desolv represent van der Waals interactions, hydrogen bonds, and hydrophobic interactions, respectively; <sup>c</sup> Final total internal energy and unbound system's energy are a pair of opposing forces that can cancel each other out; <sup>d</sup> Estimated free energy of binding is the combination of final intermolecular energy and torsional free energy.

**Table 3. Highest energy contributions for amino acid residues in AmalOBP8's binding with two volatile compounds**

Compound: Geranyl formate				
Residues	Trp106	Tyr105	Tyr46	Gly34
Energy (kJ/mol)	-2.84	-2.37	-2.11	-2.11
Compound: (Z)-3-hexenyl hexanoate				
Residues	Leu79	Leu53	Leu10	Leu50
Energy (kJ/mol)	-3.39	-2.87	-2.34	-1.98

## Figure legends

**Figure 1.** Fluorescence quenching spectra of AmalOBP8 binding with two host plant volatiles (A, geranyl formate; B, (Z)-3-hexenyl hexanoate). As the two ligands were titrated from 0 to 40  $\mu\text{mol}\cdot\text{L}^{-1}$ , the fluorescence intensity of AmalOBP8 decreased significantly.

**Figure 2.** Estimation of Stern-Volmer and Lineweaver-Burk plots for fluorescence quenching of AmalOBP8 by two host plant volatiles (A and B, Stern-Volmer equation for geranyl formate and (Z)-3-hexenyl hexanoate, respectively; C and D, Lineweaver-Burk equation for geranyl formate and (Z)-3-hexenyl hexanoate, respectively).

**Figure 3.** UV absorption spectra of AmalOBP8 in the absence and presence of two host plant volatiles (A, geranyl formate; B, (Z)-3-hexenyl hexanoate).

**Figure 4.** Structure of AmalOBP8. (A) 3D views of AmalOBP8. Seven  $\alpha$ -helices are shown as "pipes" (cylinders). (B) Amino acid sequence alignment of AmalOBP8, LmigOBP1, PregOBP56a, and CcapOBP22. A column is framed in blue if more than 70% of residues have similar physio-chemical properties.

**Figure 5.** Simulations of molecular dynamics (100 ns): (A) Fluctuations of RMSD for the AmalOBP8-geranyl formate complex. (B) Fluctuations of RMSD for the AmalOBP8-(Z)-3-hexenyl hexanoate complex. (C) Values of RMSD for geranyl formate. (D) Values of RMSD for (Z)-3-hexenyl hexanoate. (E) Plot of Rg for the AmalOBP8-geranyl formate complex. (F) Plot of Rg for the AmalOBP8-(Z)-3-hexenyl hexanoate complex. (G) Plot of residue-specific flexibility for the AmalOBP8-geranyl formate complex. (H) Plot of residue-specific flexibility for the AmalOBP8-(Z)-3-hexenyl hexanoate complex.

**Figure 6.** Analyses for the number of hydrogen bonds in AmalOBP8-ligand complexes: (A) AmalOBP8-geranyl formate complex; (B) AmalOBP8-(Z)-3-hexenyl hexanoate complex.

**Figure 7.** Patterns of molecular interactions during simulations of molecular dynamics. Views of 2D for binding of AmalOBP8 with geranyl formate (A) and (Z)-3-hexenyl hexanoate (B). Surface hydrophobicity for AmalOBP8 binding with geranyl formate (C) and (Z)-3-hexenyl hexanoate (D), respectively (dodger blue, most hydrophilic; white, intermediately hydrophobic; orange red, most hydrophobic). Electrostatic potential surface for AmalOBP8 binding with geranyl formate (E) and (Z)-3-hexenyl hexanoate (F), respectively (red, negative; white, neutral; blue, positive).

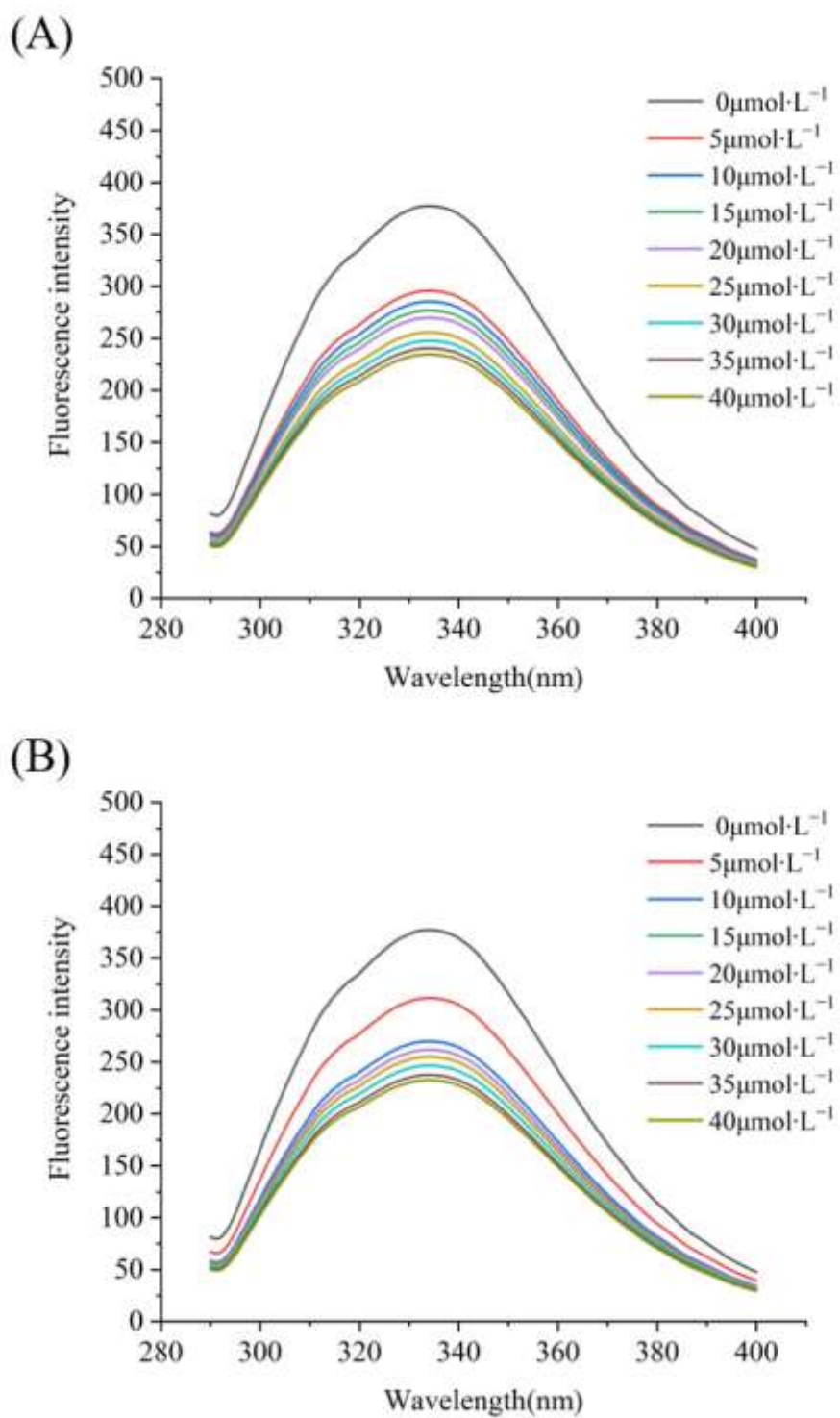


**Figure 1.** Fluorescence quenching spectra of AmalOBP8 binding with two host plant volatiles (A, geranyl formate; B, (*Z*)-3-hexenyl hexanoate). As the two ligands were titrated from 0 to 40  $\mu\text{mol}\cdot\text{L}^{-1}$ , the fluorescence intensity of AmalOBP8 decreased significantly.

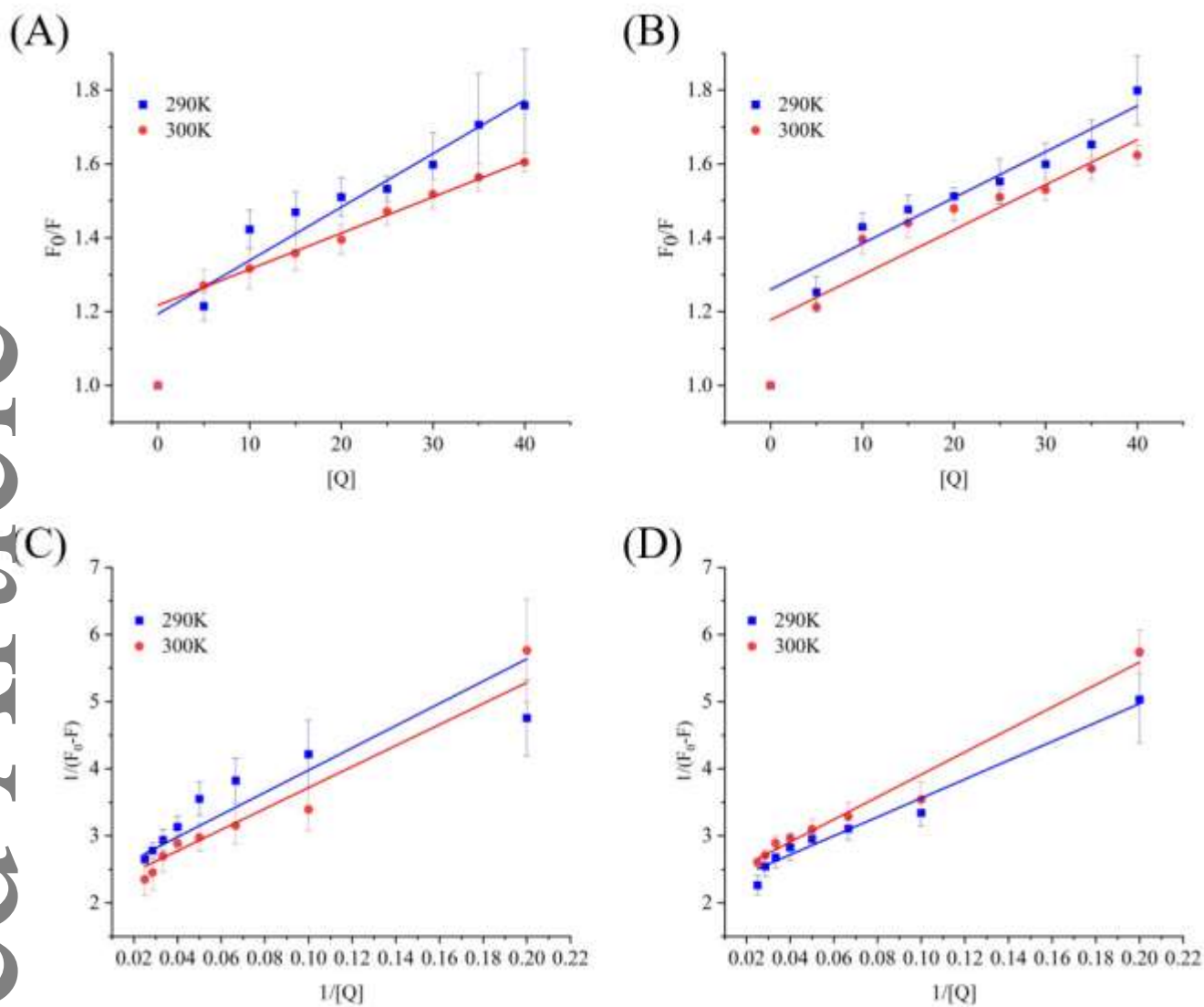


**Figure 2.** Estimation of Stern-Volmer and Lineweaver-Burk plots for fluorescence quenching of AmalOBP8 by two host plant volatiles (A and B, Stern-Volmer equation for geranyl formate and (Z)-3-hexenyl hexanoate, respectively; C and D, Lineweaver-Burk equation for geranyl formate and (Z)-3-hexenyl hexanoate, respectively).

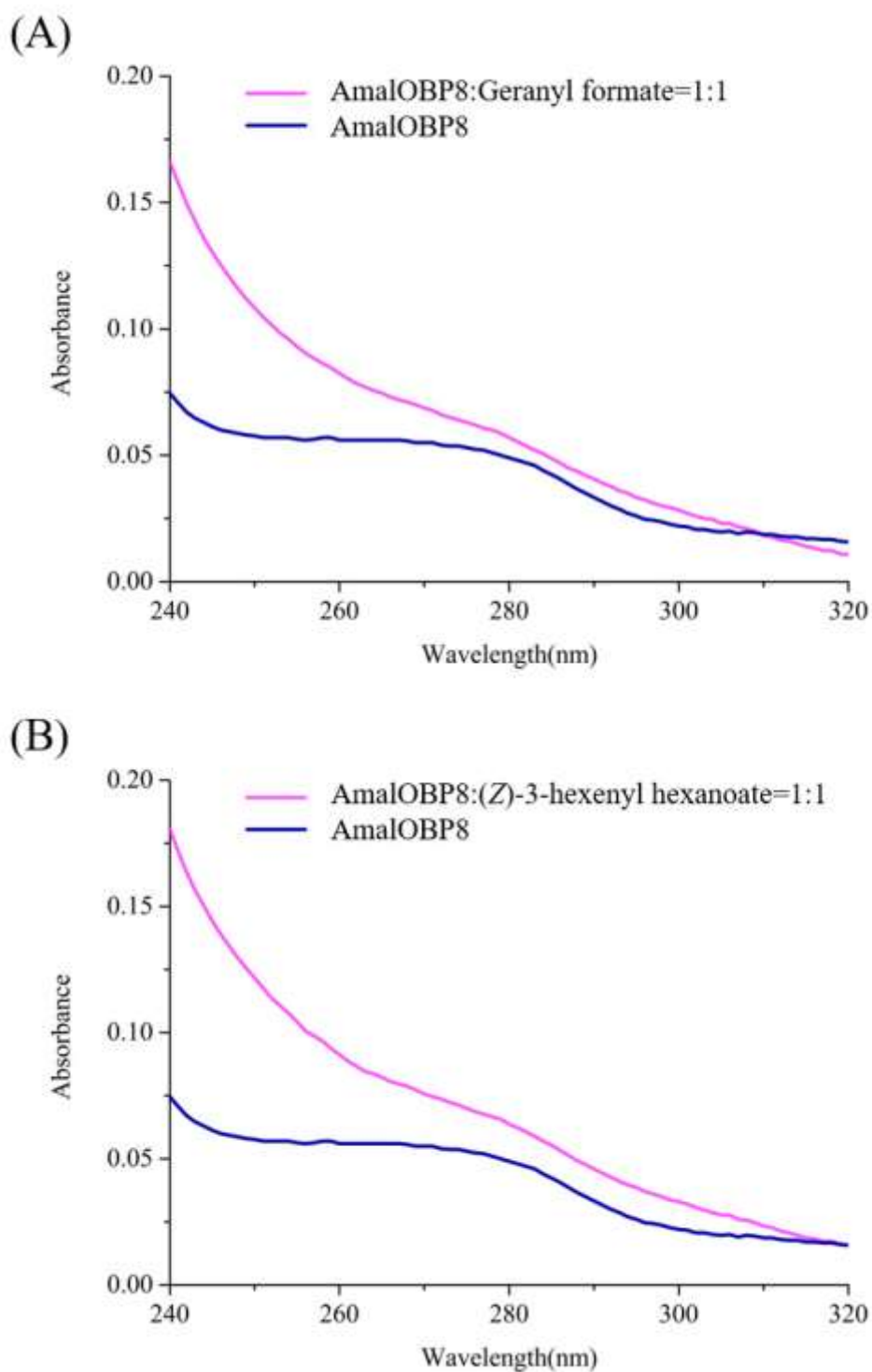


**Figure 3.** UV absorption spectra of AmalOBP8 in the absence and presence of two host plant volatiles (A, geranyl formate; B, (Z)-3-hexenyl hexanoate).



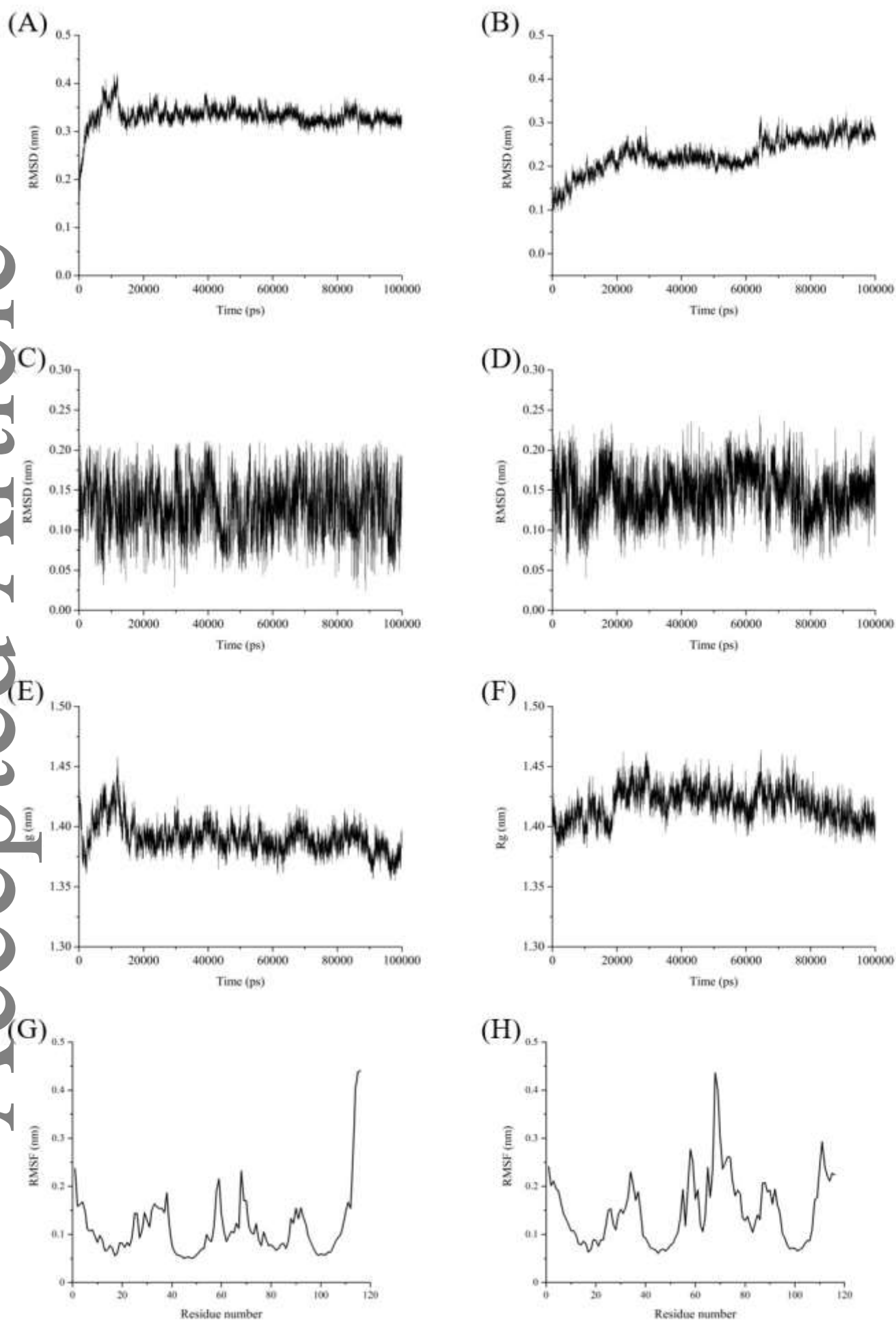


**Figure 5.** Simulations of molecular dynamics (100 ns): (A) Fluctuations of RMSD for the  
This article is protected by copyright. All rights reserved.

AmalOBP8-geranyl formate complex. (B) Fluctuations of RMSD for the AmalOBP8-(*Z*)-3-hexenyl hexanoate complex. (C) Values of RMSD for geranyl formate. (D) Values of RMSD for (*Z*)-3-hexenyl hexanoate. (E) Plot of R<sub>g</sub> for the AmalOBP8-geranyl formate complex. (F) Plot of R<sub>g</sub> for the AmalOBP8-(*Z*)-3-hexenyl hexanoate complex. (G) Plot of residue-specific flexibility for the AmalOBP8-geranyl formate complex. (H) Plot of residue-specific flexibility for the AmalOBP8-(*Z*)-3-hexenyl hexanoate complex.

Accepted Article

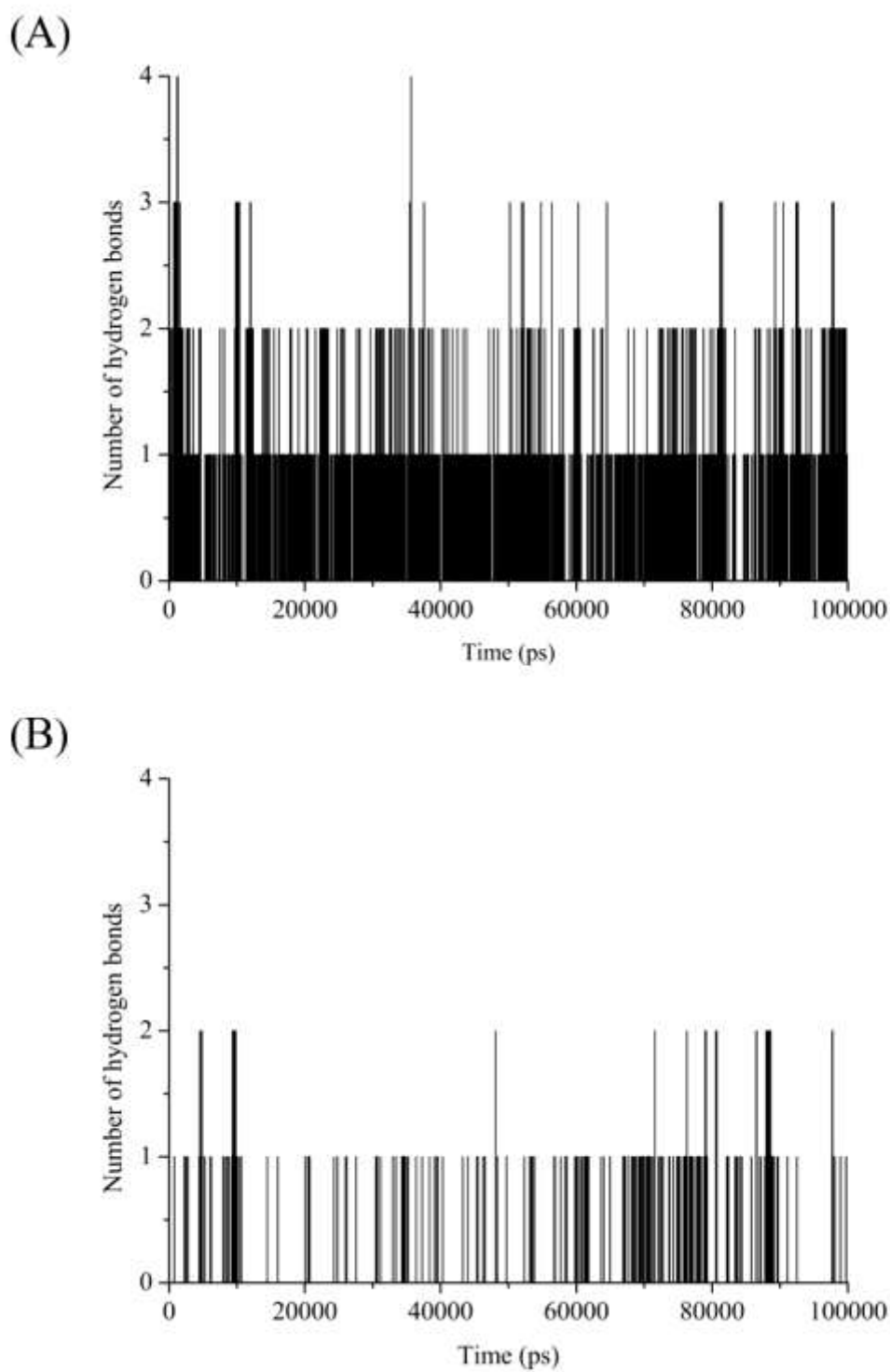


**Figure 6.** Analyses for the number of hydrogen bonds in AmalOBP8-ligand complexes: (A) AmalOBP8-geranyl formate complex; (B) AmalOBP8-(Z)-3-hexenyl hexanoate complex.

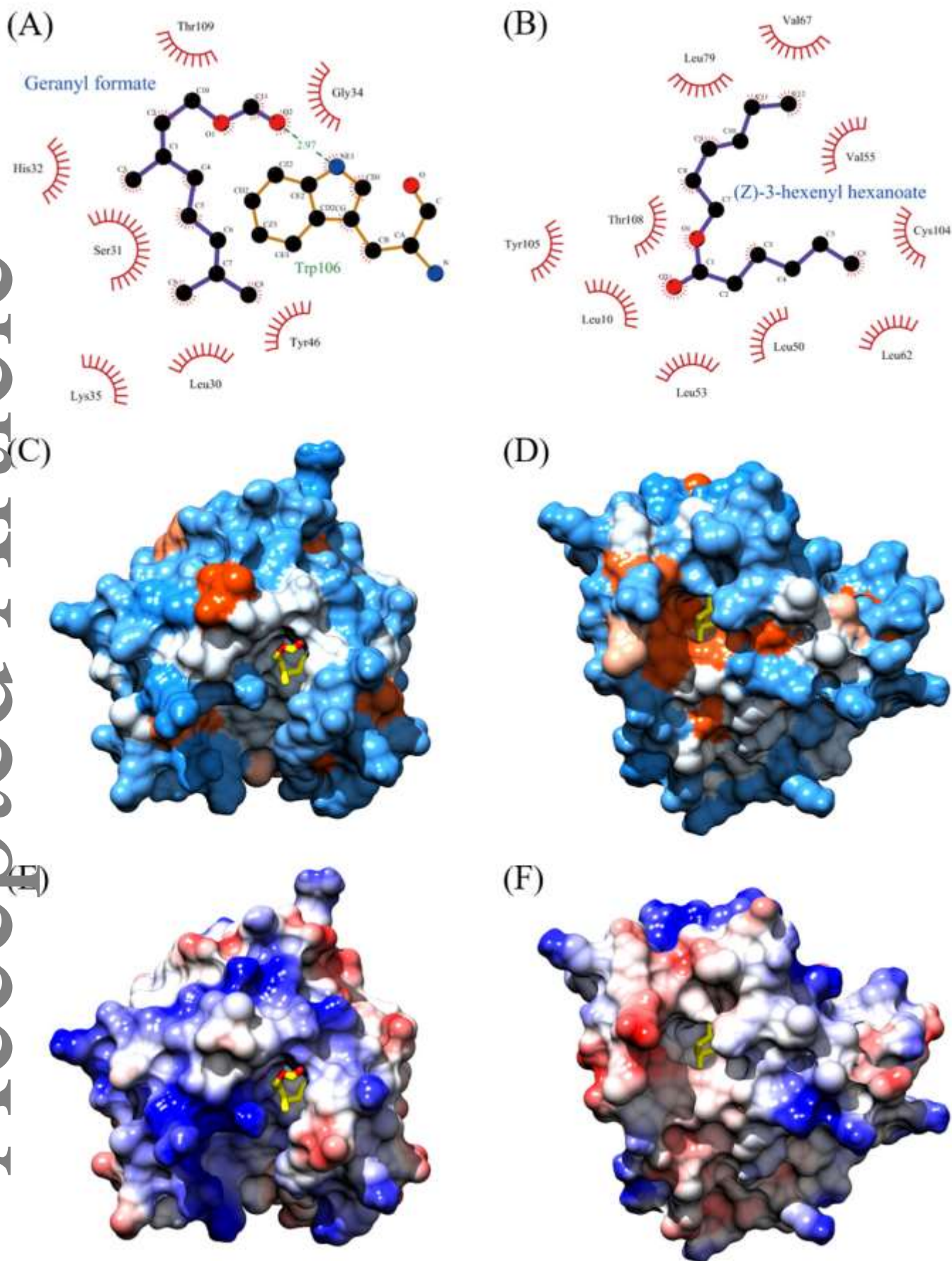


**Figure 7.** Patterns of molecular interactions during simulations of molecular dynamics. Views of 2D for binding of AmalOBP8 with geranyl formate (A) and (Z)-3-hexenyl hexanoate (B). Surface hydrophobicity for AmalOBP8 binding with geranyl formate (C) and (Z)-3-hexenyl hexanoate (D), respectively (dodger blue, most hydrophilic; white, intermediately hydrophobic; orange red, most hydrophobic). Electrostatic potential surface for AmalOBP8 binding with geranyl formate (E) and (Z)-3-hexenyl hexanoate (F),

respectively (red, negative; white, neutral; blue, positive).

Accepted Article